Spintronic properties of graphene films grown on Ni(111) substrate

S. J. Gong, Z. Y. Li, Z. Q. Yang, Cheng Gong, Chun-Gang Duan, and J. H. Chu

Articles you may be interested in

Generation of full polarization in ferromagnetic graphene with spin energy gap
Appl. Phys. Lett. **105**, 252402 (2014); 10.1063/1.4905131

Magnetization reversal and spintronics of Ni/Graphene/Co induced by doped graphene
Appl. Phys. Lett. **102**, 112403 (2013); 10.1063/1.4795764

Pt3 and Pt4 clusters on graphene monolayers supported on a Ni(111) substrate: Relativistic density-functional calculations
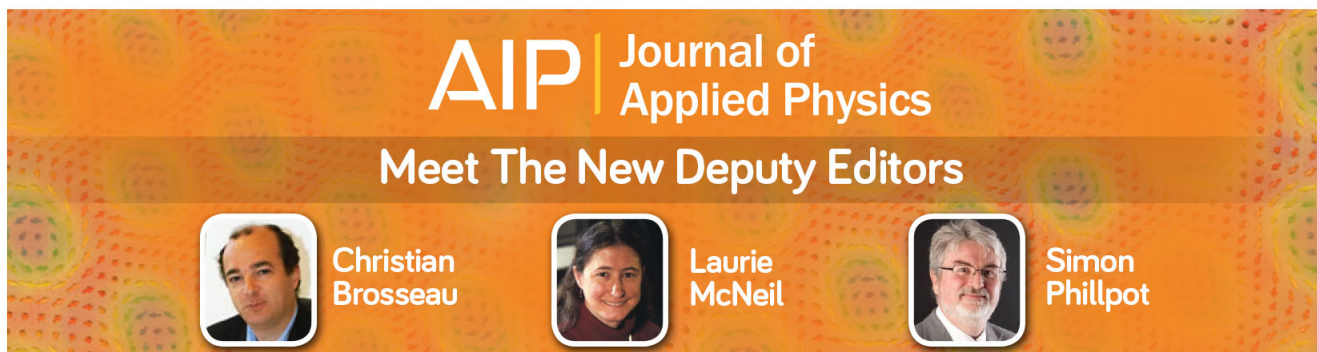J. Chem. Phys. **137**, 044710 (2012); 10.1063/1.4737885

Pt on graphene monolayers supported on a Ni(111) substrate: Relativistic density-functional calculations
J. Chem. Phys. **136**, 074701 (2012); 10.1063/1.3684891

Spintronic properties of zigzag-edged triangular graphene flakes
J. Appl. Phys. **108**, 074301 (2010); 10.1063/1.3489919

Spintronic properties of graphene films grown on Ni(111) substrate

S. J. Gong,[1,2,a)] Z. Y. Li,[3] Z. Q. Yang,[4] Cheng Gong,[5] Chun-Gang Duan,[1] and J. H. Chu[1,2]

[1]*Key Laboratory of Polar Materials and Devices, Ministry of Education, East China Normal University, Shanghai 200241, People's Republic of China*
[2]*National Laboratory for Infrared Physics, Shanghai Institute of Technical Physics, Chinese Academy of Sciences, Shanghai 200083, People's Republic of China*
[3]*College of Science, University of Shanghai for Science and Technology, Shanghai 200093, People's Republic of China*
[4]*National Laboratory for Surface Physics, Fudan University, Shanghai 200433, People's Republic of China*
[5]*Department of Materials Science & Engineering, University of Texas at Dallas, Richardson, Texas 75080, USA*

Graphene is believed to be a promising candidate for spintronic applications. In this study, we investigate the electronic, magnetic, and, especially, spintronic properties of graphene films grown on Ni(111) substrate using relativistic density-functional calculations. Enhanced Rashba spin-orbit coupling (SOC), with a magnitude of up to 20 meV—several orders of magnitude larger than the intrinsic SOC strength in freestanding graphene—is found at the graphene–Ni(111) interface. The hybridization between graphene's p_z states and Ni's $3d$ states magnetizes the interfacial carbon atoms and induces a sizable exchange splitting in the π band of the graphene sheet. The calculated results agree well with the recently reported experimental data and provide a deep understanding of the spintronic behavior of graphene in contact with a $3d$-ferromagnet. © 2011 American Institute of Physics. [doi:10.1063/1.3622618]

INTRODUCTION

Recently, spin-orbit couplings[1,2] (SOCs) have attracted considerable attention in the field of spintronics due to the advantage of their enabling the manipulation of the spin degree of freedom even without the requirement of externally applied magnetic fields.[3–5] Various all-electrical-operation spin functional devices have been proposed based on SOCs, such as the well-known Datta-Das spin field-effect-transistor,[3] spin filters,[6] spin valves,[7] spin interference,[8] spin qubit gates,[9,10] etc. Among the varieties of SOCs, the Rashba SOC,[2] which arises from structure inversion asymmetry, wins the most research interest because its strength can be flexibly modulated, for example, by gate voltage[11] or surface doping.[12] The Rashba Hamiltonian $H_R = \alpha (\mathbf{p} \times \sigma) \cdot \mathbf{E}$; α represents the Rashba strength parameter, σ is the Pauli spin operator, $\mathbf{p} = \hbar\mathbf{k}$ is the momentum of the electron, and $\mathbf{E}$ is the electric field, which introduces an effective magnetic field perpendicular to the wavevector $\mathbf{k}$. The existence of the interface/surface always introduces inversion symmetry breaking, thus producing the Rashba SOC.[13,14]

Graphene, a two-dimensional carbon hexagonal crystal,[15] has been considered as a promising candidate material for spintronic applications[16] since its discovery in 2004. The SOCs in graphene have been attracting ever more research efforts.[17–24] Generally, SOCs in graphene are classified into two categories: intrinsic[17–19] and extrinsic components.[22,23] The former is allowed by crystal symmetry, and the latter relies on inversion symmetry breaking.[25,26] Kane and Mele

are the first to have reported on the intrinsic SOC in graphene, which was believed to open a gap of about 0.1 meV and thus induce a quantum spin Hall effect (QSHE) in graphene nanoribbon.[17] Subsequently, the spin-orbit gap was reexamined by Yao *et al.*, and a much smaller gap (0.00086 meV) was obtained in their *ab initio* calculations,[18] which means the QSHE proposed by Kane and Male could hardly be observed unless the temperature were as low as $T \leq 10^{-2}$ K. Such weak intrinsic SOC in graphene is believed to be impractical for effectively manipulating electron spin,[27] which makes it essential to explore large extrinsic SOC. Many approaches have been tried in order to enhance the extrinsic SOC strength in graphene—for example, applying gate voltage,[19] introducing impurities,[21] curving the graphene plane,[28] building interfaces by depositing graphene on substrates,[22–24] etc. The most exciting finding is that an extraordinarily large spin splitting energy of 225 meV was detected in the graphene/Ni(111) system by means of angle-resolved photoemission spectroscopy,[22] which makes the graphene–Ni interface one of the hottest research subjects. Rader *et al.* reexamined the same system using *spin-* and angle-resolved photoemission spectroscopy.[23] They revealed, however, distinctly different spin splitting behaviors. The total of the Rashba and exchange splittings they obtained was less than 45 meV. Very recently, the induced magnetism of carbon atoms at the graphene–Ni(111) interface was observed by using x-ray magnetic circular dichroism.[29] All these interesting and controversial experimental findings stimulated us to make a theoretical investigation in order to better understand the graphene/3d-ferromagnet contact.

a)Author to whom correspondence should be addressed. Electronic mail: sjgong@ee.ecnu.edu.cn.

In this paper, we study the systems of graphene films grown on Ni(111) substrate using first-principles calculations based on relativistic density-functional theory (DFT). The electronic, magnetic, and, especially, spintronic properties of the graphene/Ni(111) system are discussed. We obtain Rashba and exchange spin splittings in the π band of the graphene sheet, which directly contacts the Ni(111) surface. The calculated Rashba splitting energy is found to be linearly dependent on the wave vector, and its magnitude reaches 20 meV, which is several orders of magnitude larger than the reported intrinsic SOC.[17,18] The hybridization between graphene's p_z states and Ni's $3d$ states results in sizable exchange splitting in the π band of the graphene sheet and the experimentally observable magnetism of carbon atoms at the graphene–Ni(111) interface.[29] The calculated results are in accord with the recent experimental findings[23,29] and provide a theoretical understanding of the graphene/$3d$-frromagnet contact.

FIG. 1. Schematic of three-layer graphene film grown on a six-layer Ni(111) substrate.

MODELS AND METHODS

The calculations are performed by using the projector augmented wave (PAW) formalism of the DFT as implemented in the Vienna *ab initio* simulation package[30] and include spin-orbit coupling. Because the generalized gradient approximation[31] gives essentially no bonding between graphene planes and leads to excessively large bilayer spacing,[32] we perform the calculations within the localized density approximation and get the reasonable bilayer distance of 3.34 Å, which is in good agreement with the experimental value. An energy cutoff of 500 eV for the plane-wave expansion of the PAWs is used, and the Brillouin zone (BZ) is sampled by using a $37 \times 37 \times 1$ Γ centered k-point grid. For geometry optimization, all of the internal coordinates are relaxed until the Hellmann-Feynman forces are less than 0.03 eV/Å. A Ni lattice is mapped onto graphene's 1 * 1 unit cell, and structural relaxation with a fixed lattice constant of Ni shows that the lattice constant mismatch leads to the 1.2% stretching of the graphene's lattice. The reverse matching procedure, in which Ni(111) is set to lattice match graphene, produces no noticeable difference in the calculated results. The vacuum thickness along the z-axis is 20 Å, which is enough to avoid interaction between adjacent supercells.

The structure model for the graphene/Ni(111) system has been discussed in many DFT studies, and the adsorption configuration, in which one carbon atom is positioned on top of a surface Ni atom, is regarded as the most stable configuration.[33,34] The equilibrium interfacial spacing between the graphene layer and the Ni surface is about 2.0 Å. Figure 1(a) shows a side view of the graphene/Ni(111) contact in which three layers of graphene and six layers of Ni stacking are considered. It is found that the relaxed geometry of the substrate is influenced only by the first graphene sheet. Neither the substrate nor the first graphene layer is altered when subsequent graphene layers are added. Although the added graphene layers do not influence the interfacial properties we are concerned wit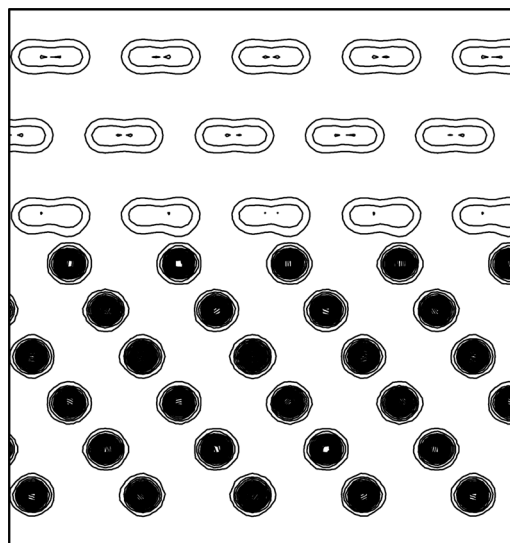h, they provide helpful information for better understanding the graphene/Ni(111) system, as is illustrated in the following section.

RESULTS AND DISCUSSION

The calculated band structures of the graphene/Ni(111) systems are shown in Fig. 2, in which Γ, **K**, and **M** are the high symmetry **k** points. One-, two-, and three-layer graphene films are considered and are shown in Figs. 2(a), 2(b), and 2(c), respectively. For each system, we show only the majority spin band structure, which provides sufficient information. It is known that Dirac point and linear energy dispersion are characteristic of freestanding monolayer graphene, and parabolic dispersion is an aspect of pure bilayer graphene. As is shown in Fig. 2(a), the characteristic band structure of the monolayer graphene is seriously destroyed by the strong interfacial interaction. This one-layer-graphene/Ni(111) system has been previously investigated elsewhere[35] and was reexamined here only for comparison with two other systems. With two-layer graphene film, the Dirac point and linear energy dispersion are partially recovered. The recovered part is contributed by the second graphene layer, from which we can infer that the bottom graphene layer, which strongly interacts with the Ni surface, decouples with the second graphene sheet. A critical point is that the Dirac point obtained here is about 0.35 eV below the Fermi level, indicating that the bilayer graphene film is n-doped by the Ni substrate. In three-layer graphene film, the characteristic band structure of the bilayer graphene appears. Different from the pure bilayer graphene, an energy gap is observed in Fig. 2(c). It is believed that the energy gap is induced by the electrostatic potential difference between the above two graphene layers introduced by the charge redistribution at the interface. The red (gray) curves in Fig. 2(c) represent the band structure of the pure bilayer graphene with a gate electric field of about E = 0.6 V/nm, through which the induced electrostatic potential difference can be quantitatively
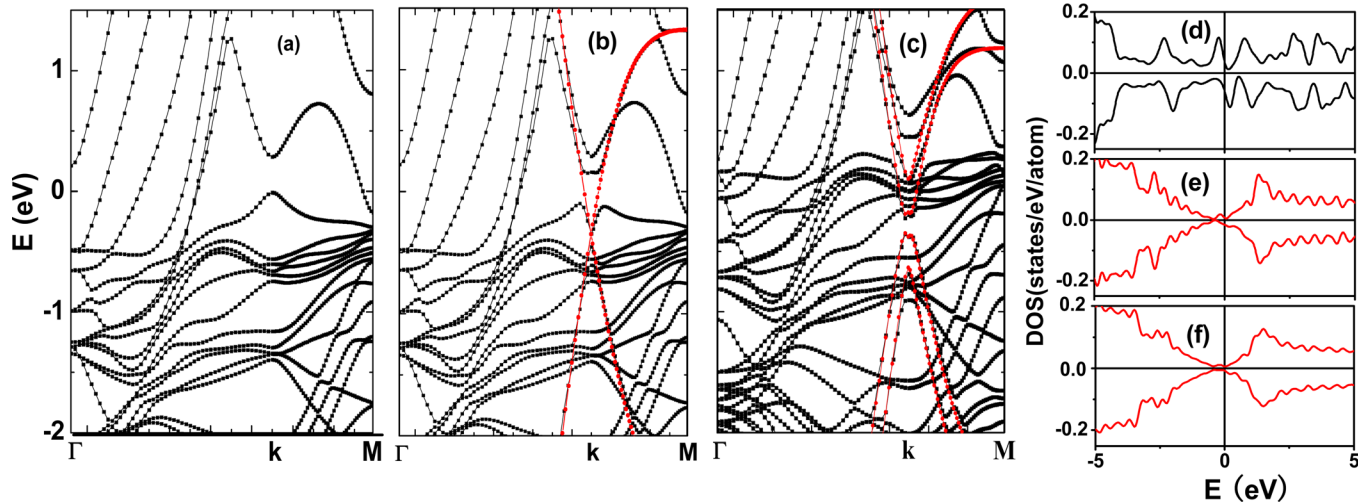
FIG. 2. (Color online) Majority-spin band structures of the one-layer (a), two-layer (b), and three-layer (c) graphene films grown on Ni(111) substrate. The red (gray) curves in (b) represent the band structure of the pure monolayer graphene, the energy level of which is purposely lowered to fit with the Ni-doped graphene's bands. The red (gray) curves in (c) represent the band structure of the pure bilayer graphene with a gate electric field E = 0.6 V/nm. (d) The spin resolved DOS of the graphene monolayer in the one-layer-graphene/Ni(111) system. (e) The spin resolved DOS of the top graphene layer in two-layer-graphene/Ni(111) system. (f) The spin resolved DOS of the top two graphene layers in the three-layer-graphene/Ni(111) system.

estimated. In addition, we also plot the spin resolved density of states (DOS) of carbon atoms for the three systems, as shown in Figs. 2(d)-2(f), respectively. Figure 2(d) shows the DOS of the graphene monolayer of the one-layer-graphene/Ni system. It can be clearly seen that the carbon atoms are magnetized and the DOS is very different from that of the freestanding graphene monolayer. Figure 2(e) shows the DOS of the top graphene layer of the two-layer-graphene/Ni system. The Dirac point, at which both the spin-up and the spin-down DOS are zero, is clearly observed at the left side of the Fermi level. Figure 2(f) shows the DOS of the top two graphene layers of the three-layer-graphene/Ni system. Comparing the spin resolved DOS shown in Figs. 2(d)-2(f), we can easily find that only the graphene layer directly contacting the Ni surface is seriously influenced by the

substrate. In fact, we also plotted the spin resolved DOS of the bottommost graphene layer in the two-layer-graphene/Ni and three-layer-graphene/Ni systems, and these plots do not show much difference from that of the one-layer-graphene/Ni system and are not shown in the manuscript. This means the added graphene layers do not influence the interfacial properties.

When dealing with the Rashba and exchange spin splitting energy, we consider the same conditions as those reported in the experiments,[22,23] i.e., the measured wavevector **k** along the $\overline{\Gamma M}$ vector and the electric field **E** along the normal direction of the graphene–Ni(111) interface. It is found that only in the π band of the graphene sheet, which directly contacts the Ni(111) surface, are Rashba and exchange spin splittings obtained, and the subsequent
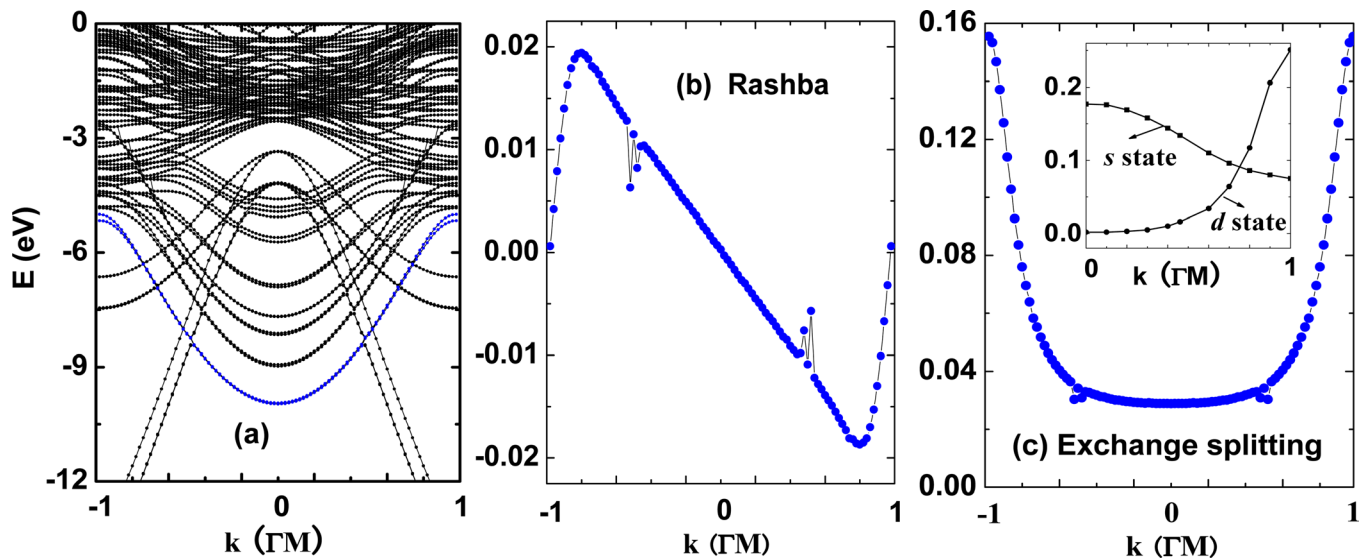

FIG. 3. (Color online) (a) Band structure of the two-layer-graphene/Ni(111) system, in which spin-up and spin-down π bands of the bottom graphene sheet are plotted as blue (gray) dotted curves. (b) Rashba and (c) exchange splitting energy obtained in π bands of the bottom graphene layer. The inset in (c) shows the components of the s and d states of Ni atoms in the bottom graphene's π bands.

graphene layers have little impact on them. As can be inferred from the Rashba Hamiltonian, the symmetry of the energy bands under the $\mathbf{k} \rightarrow -\mathbf{k}$ operator will be destroyed, and the Rashba spin splitting energy is linearly dependent on the wavevector $\mathbf{k}$. We show the band structure of the two-layer-graphene/Ni(111) system in Fig. 3(a), in which the spin-up and spin-down π bands of the graphene sheet are plotted as blue (gray) curves. The calculated data of Fig. 3(a) reveal that both Rashba and exchange spin splittings are present in the π bands of the graphene sheet, which is, however, hard to see clearly in Fig. 3(a). To get the individual magnitudes of the Rashba and exchange splitting energies, we do calculations twice for the same system: one with SOC, and the other without SOC. If the SOC is included in the calculation, the energy difference between the spin-up ($E_\uparrow$) and spin-down ($E_\downarrow$) gives the total spin splitting energy $\Delta E_{exc+Rash} = E_\uparrow - E_\downarrow$. If not, it gives only the exchange splitting ΔE_{exc}. By doing these, we separate the Rashba and exchange splitting energies, which are clearly illustrated in Figs. 3(b) and 3(c), respectively. As can be seen in Fig. 3(b), the obtained Rashba spin splitting energy with a maximal magnitude of about 20 meV shows a perfectly linear relation with the wavevector, except that at the boundary of the BZ it decreases to zero because of the periodic boundary condition used in the simulation. The exchange spin splitting in the center of the BZ is less than 30 meV; however, it sharply increases to about 150 meV at the boundary of the BZ. The extraordinarily large exchange splitting energy is contributed by the strong hybridization of Ni's 3d states. The inset in Fig. 3(c) shows components of the s and d states of Ni atoms hybridized in graphene's π bands. From the Γ to the M point, the component of Ni's d states undergoes an obvious increase, whereas that of the s states smoothly decreases. According to Rader *et al.*'s report,[23] the total spin splitting energy $|\Delta E_{Rash+Exch}|$ was less than 45 meV at the wavevector 0.7 $\mathring{A}^{-1}$. At their examined wavevector, i.e., 0.5 in the x-coordinate in Fig. 3, the Rashba splitting energy is found to be about 10 meV, and the exchange splitting is about 34 meV; these values are in good agreement with the experimental claims.

Very recently, the induced magnetism of carbon atoms at the graphene–Ni(111) interface was reported in experiments.[29] In the present calculations, we also get such magnetism at the interfacial carbon atoms. Distributions of the spin density on the graphene sheet are plotted in Fig. 4, in which A and B represent the two sublattices of graphene. As can be clearly seen, the spin distribution is sublattice-dependent, and the magnetization at sublattice A ($\sim 0.03 \ \mu_B$) is obviously stronger than that at sublattice B ($\sim -0.01 \ \mu_B$). It is interesting to note that although the carbon atoms at sublattice B directly contact the Ni atoms at the interface and get electrons from the Ni substrate, the induced magnetism dominates at sublattice A. We also investigate the distribution of the magnetic moments of Ni atoms. From the topmost to the bottommost layer of the Ni(111) substrate, the magnetic moments in order are 0.46, 0.54, 0.58, 0.61, 0.64, and 0.65 μ_B. It is clear that Ni atoms at the interface have the smallest magnetic moment because of the hybridization effect.
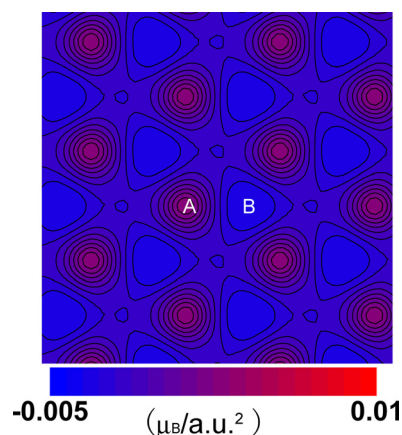

FIG. 4. (Color online) The calculated spin density distribution on the graphene sheet.

CONCLUSIONS

In summary, graphene films grown on Ni(111) substrate are investigated using DFT calculations. The electronic, magnetic, and spintronic properties of this complex system are discussed. Both Rashba and exchange spin splittings are obtained in the π bands of the graphene sheet, which directly contacts the Ni(111) substrate. The Rashba spin splitting is found to be linearly dependent on the wavevector, with a magnitude of up to 20 meV. The hybridization between graphene's p_z states and Ni's 3d states results in sizable exchange splitting in the π band of the graphene sheet and the experimentally observable magnetism of carbon atoms at the interface. Our investigations not only help one to understand graphene/3d-ferromagnet contact, but also confirm some of the present experimental observations.

ACKNOWLEDGMENTS

[1]G. Dresselhaus, Phys. Rev. **100**, 580 (1955).
[2]Y. A. Bychkov and E. I. Rashba, J. Phys. C **17**, 6039 (1984).
[3]S. Datta and B. Das, Appl. Phys. Lett. **56**, 665 (1990).
[4]D. Stepanenko and N. E. Bonesteel, Phys. Rev. Lett. **93**, 140501 (2004).
[5]J. Wunderlich, B. Kaestner, J. Sinova, and T. Jungwirth, Phys. Rev. Lett. **94**, 047204 (2005).
[6]S. J. Gong and Z. Q. Yang, J. Appl. Phys. **102**, 033706 (2007).
[7]F. Mireles and G. Kirczenow, Phys. Rev. B **66**, 214415 (2002).
[8]D. Frustaglia and K. Richter, Phys. Rev. B **69**, 235310 (2004).
[9]S. J. Gong and Z. Q. Yang, Phys. Lett. A **367**, 369 (2007).
[10]P. Földi, B. Molnár, M. G. Benedict, and F. M. Peeters, Phys. Rev. B **71**, 033309 (2005).
[11]J. Nitta, T. Akazaki, H. Takayanagi, and T. Enoki, Phys. Rev. Lett. **78**, 1335 (1997).
[12]E. Frantzeskakisa, A. Crepaldia, S. Ponsa, K. Kerna, and M. Grionia, J. Electron Spectrosc. Relat. Phenom. **181**, 88 (2010).
[13]S. LaShell, B. A. McDougall, and E. Jensen, Phys. Rev. Lett. **77**, 3419 (1996).

[14]K. S. Cho, C. T. Liang, Y. F. Chen, and J. C. Fan, Semicond. Sci. Technol. **22**, 870 (2007).

[15]K. S. Novoselov, A. K. Geim, S. V. Morozov, D. Jiang, Y. Zhang, S. V. Dubonos, I. V. Grigorieva, and A. A. Firsov, Science **306**, 666 (2004).

[16]E. W. Hill, A. K. Geim, K. Novoselov, F. Schedin, and P. Blake, IEEE Trans. Magn. **42**, 2694 (2006).

[17]C. L. Kane and E. J. Mele, Phys. Rev. Lett. **95**, 226801 (2005); **95**, 146802 (2005).

[18]Y. Yao, F. Ye, X. L. Qi, S. C. Zhang, and Z. Fang, Phys. Rev. B **75**, 041401(R) (2007).

[19]R. van Gelderen and C. M. Smith, Phys. Rev. B **81**, 125435 (2010).

[20]H. Min, J. E. Hill, N. A. Sinitsyn, B. R. Sahu, L. Kleinman, and A. H. MacDonald, Phys. Rev. B **74**, 165310 (2006).

[21]A. H. Castro Neto and F. Guinea, Phys. Rev. Lett. **103**, 026804 (2009).

[22]Y. S. Dedkov, M. Fonin, U. Rüdiger, and C. Laubschat, Phys. Rev. Lett. **100**, 107602 (2008).

[23]O. Rader, A. Varykhalov, J. Sánchez-Barriga, D. Marchenko, A. Rybkin, and A. M. Shikin, Phys. Rev. Lett. **102**, 057602 (2009).

[24]I. Gierz, J. H. Dil, F. Meier, B. Slomski, J. Osterwalder, J. Henk, R. Winkler, C. R. Ast, and K. Kern, e-print arXiv: 1004.1573.

[25]E. I. Rashba, Phys. Rev. B **79**, 161409 (2009).

[26]D. Huertas-Hernando, F. Guinea, and A. Brataas, Phys. Rev. B **74**, 155426 (2006).

[27]Y. G. Semenov, K. W. Kim, and J. M. Zavada, Appl. Phys. Lett. **91**, 153105 (2007).

[28]D. Huertas-Hernando, F. Guinea, and A. Brataas, Phys. Rev. B **74**, 155426 (2006).

[29]M. Weser, Y. Rehder, K. Horn, M. Sicot, M. Fonin, A. B. Preobrajenski, E. N. Voloshina, E. Goering, and Yu. S. Dedkov, Appl. Phys. Lett. **96**, 012504 (2010).

[30]G. Kresse and J. Furthmuller, Comput. Mater. Sci. **6**, 15 (1996); Phys. Rev. B **54**, 11169 (1996).

[31]J. P. Perdew, K. Burke, and M. Ernzerhof, Phys. Rev. Lett. **77**, 3865 (1996).

[32]D. W. Boukhvalov and M. I. Katsnelson, Phys. Rev. B **78**, 085413 (2008).

[33]V. M. Karpan, G. Giovannetti, P. A. Khomyakov, M. Talanana, A. A. Starikov, M. Zwierzycki, J. van den Brink, G. Brocks, and P. J. Kelly, Phys. Rev. Lett. **99**, 176602 (2007).

[34]Y. Gamo, A. Nagashima, M. Wakabayashi, M. Terai, and C. Oshima, Surf. Sci. **374**, 61 (1997).

[35]G. Giovannetti, P. A. Khomyakov, G. Brocks, V. M. Karpan, J. van den Brink, and P. J. Kelly, Phys. Rev. Lett. **101**, 026803 (2008).